PERGAMON

Journal of the Mechanics and Physics of Solids
49 (2001) 1937–1950

JOURNAL OF THE
MECHANICS AND
PHYSICS OF SOLIDS

www.elsevier.com/locate/jmps

Dynamics of nanoscale pattern formation of an epitaxial monolayer

W. Lu, Z. Suo *,[1]

Mechanical and Aerospace Engineering Department and Princeton Materials Institute, Princeton University, Princeton, NJ 08544, USA

Abstract

A two-phase monolayer grown on an elastic substrate may form stripes or dots on the scale of nanometers. Sometimes these stripes and dots order into superlattices. This paper reports on a simulation on the basis of a model proposed by the authors recently. The size selection and spatial ordering result from two competing actions: the phase boundary energy tends to coarsen the phases, and the concentration-dependent surface stress tends to refine the phases. A nonlinear diffusion equation couples the concentration field in the epilayer and the stress field in the substrate. The simulation reveals remarkably rich dynamics. An epilayer may evolve into various patterns, suggesting a significant degree of experimental control in growing nanoscale superlattices, just as in growing atomic crystals.

Keywords: Nanostructure; Surface stress; Epitaxial film; Self-assembly; Phase field model

1. Introduction

On a solid surface an epitaxial monolayer can form various two dimensional patterns (Fig. 1). Kern et al. (1991) found that on a Cu(110) surface submonolayer oxide forms periodic stripes about 10 nm wide, running in the $\langle 0\,0\,1\rangle$ direction, and stable on annealing. Upon depositing a mixture of S and Ag on a Ru(0 0 0 1) surface, Pohl et al. (1999) obtained a triangular superlattice of S rich dots in a Ag matrix. Not all two-phase monolayers form superlattices. Irregular arrangements like those in Figs. 1c and 1d have often been observed (Röder et al., 1993; Clark and Friend, 1999).

* Tel.: +1-609-258-0250; fax: +1-609-258-6123.
E-mail address: suo@princeton.edu (Z. Suo).
[1] www.princeton.edu/∼suo

0022-5096/01/$ - see front matter
PII: S0022-5096(01)00023-0

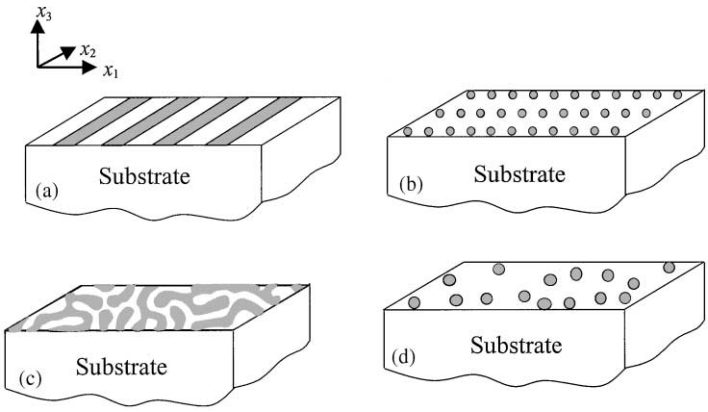

Fig. 1. Self-organized nanoscale patterns of an epilayer on a solid surface.

Even for these irregular arrangements, the phase sizes often stabilize on the nanoscale (1–100 nm). Two questions arise. What sets the length scale of the phases? Why do they self-assemble into superlattices?

If a bulk two-phase alloy is annealed, allowing atoms to diffuse, phases will coarsen to reduce the total area of phase boundary. Time permitting, coarsening will continue until only one large particle is left in a matrix. For a two-phase epilayer, the observed size selection suggests that, in addition to the phase coarsening action, a phase refining action should exist. Surface stress can provide such a refining action (Alerhand, et al., 1988; Lu and Suo, 1999). For a non-uniform surface, the surface stress is also nonuniform, causing a fringe elastic field in the substrate. When the phase size is reduced, the fringe field depth is also reduced, and so is the elastic energy. It is this reduction in the elastic energy that drives phase refining. The two competing actions—coarsening due to phase boundaries and refining due to surface stress—can select an equilibrium phase size. Furthermore, a superlattice of dots or stripes may minimize the total free energy, so that the competing actions also drive the self-assembly into the superlattices (Ng and Vanderbilt, 1995).

From the above discussion, it is clear that a model of the nanoscale self-assembly should contain the following ingredients: phase separation, phase coarsening, and phase refining. Each ingredient may be given alternative theoretical representations. We have proposed a continuous phase model (Suo and Lu, 2000). The model represents a phase boundary by a concentration gradient, analogous to the work of Cahn and Hilliard (1958) on spinodal decomposition. Other structural transformations have also been simulated this way; see Chen and Wang (1996) for reviews. In particular, Chen and Khachaturyan (1993) included the long-range Coulomb interaction, which helps to order the phases.

Previous studies on two-phase epilayers (e.g., Ng and Vanderbilt, 1995; Ibach, 1997) have focused on the energetics of the superlattices. The continuous phase field model allows us to study the dynamic process of growing a superlattice from a disordered

initial concentration distribution. This is of great consequence in a system of many equilibrium configurations due to translational and rotational symmetries. To investigate the stability of the uniform concentration field, we carried out a linear perturbation analysis (Lu and Suo, 1999). We obtained the condition under which concentration perturbation will grow, and the wavelength of the fastest growth mode. This paper builds on our previous papers and describes a simulation of the entire self-assembly process. We show that given a random initial concentration field, the two phases rapidly approach the equilibrium sizes, but slowly order into a superlattice. On the other hand, if the symmetry is broken, either by the initial conditions or by material anisotropy, spatial ordering greatly accelerates. The simulation suggests a significant degree of experimental control in growing nanoscale superlattices.

2. The continuous phase field model

This section summarizes the continuous phase field model. Readers familiar with out previous papers (Suo and Lu, 2000, 2001) may skip this section. Imagine an epilayer of two atomic species A and B on a substrate of atomic species S. The two species A and B can be both different from that of the substrate (such as sulfur–silver mixture on a ruthenium substrate). Alternatively, only one species of the epilayer is different from that of the substrate (such as oxygen atoms on a copper substrate). For simplicity, we assume that the epilayer is a substitutional alloy of A and B. Atomic diffusion is restricted within the epilayer. As shown in Fig. 1, the substrate occupies the half-space $x_3 < 0$, bounded by the x_1–x_2 plane.

The free energy of the system consists of two parts: the surface and the bulk, namely,

$$G = \int_A \Gamma \, \mathrm{d}A + \int_V W \, \mathrm{d}V, \tag{1}$$

where Γ is the surface energy per unit area of the epilayer, and W is the elastic energy per unit volume of the substrate. Both area A and volume V are measured in the undeformed configuration of an infinite substrate.

The elastic energy density, W, takes the usual form, being quadratic in the strain tensor, ε_{ij}. A Latin subscript runs from 1 to 3. The strain tensor ε_{ij} relates to the displacement gradient tensor in the usual way:

$$\varepsilon_{ij} = \tfrac{1}{2}(u_{i,j} + u_{j,i}). \tag{2}$$

We assume that the substrate is elastically isotropic, so that

$$W = \frac{E}{2(1+v)} \left[\varepsilon_{ij}\varepsilon_{ij} + \frac{v}{1-2v} (\varepsilon_{kk})^2 \right], \tag{3}$$

where E is Young's modulus and v is Poisson's ratio. The summation convention over a repeated subscript is adopted.

In our model the surface energy density, Γ, takes an unusual form. Let concentration C be the fraction of atomic sites on the surface occupied by species B. Regard the concentration as a time-dependent, spatially continuous function, $C(x_1, x_2, t)$. Assume that Γ is a function of the concentration C, the concentration gradient $C_{,\alpha}$, and the

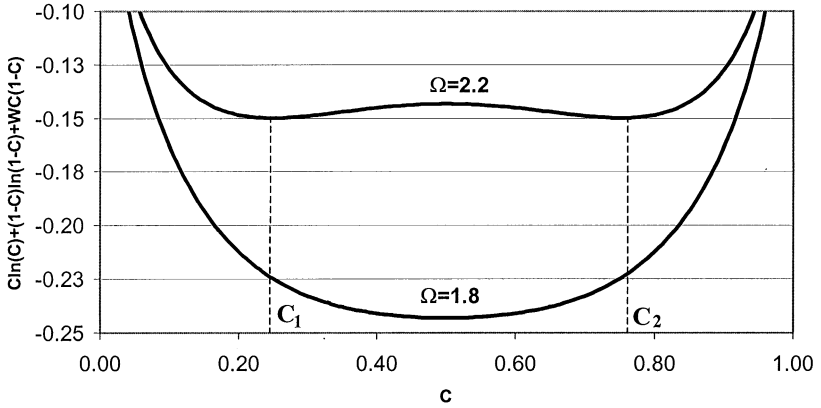

Fig. 2. The curve of $C\ln C+(1-C)\ln(1-C)+\Omega C(1-C)$ can have one or two wells for different Ω.

strain in the surface, $\varepsilon_{\alpha\beta}$. A Greek subscript runs from 1 to 2. Expand the function $\Gamma(C, C_{,\alpha}, \varepsilon_{\alpha\beta})$ to the leading-order terms in the concentration gradient $C_{,\alpha}$ and the strain $\varepsilon_{\alpha\beta}$:

$$\Gamma = g + hC_{,\beta}C_{,\beta} + f\varepsilon_{\beta\beta}, \tag{4}$$

where g, f and h are all functions of the concentration C. We have assumed isotropy in the plane of the surface; otherwise both f and h should be replaced by second rank tensors. The leading-order term in the concentration gradient is quadratic because, by symmetry, the term linear in the concentration gradient does not affect the surface energy. We have neglected the terms quadratic in the displacement gradient tensor, which relate to the excess in the elastic stiffness of the epilayer relative to the substrate. We next explain the physical content of Eq. (4) term by term.

When the concentration field is uniform in the epilayer, the substrate is unstrained, and the function $g(C)$ is the only remaining term; it represents the surface energy per unit area of the uniform epilayer on the unstrained substrate. To describe phase separation, we may prescribe $g(C)$ as any function with double wells. In numerical simulation, we assume that the epilayer is a regular solution so that the function takes the form

$$g(C) = g_{\mathrm{A}}(1-C) + g_{\mathrm{B}}C + \Lambda kT[C\ln C + (1-C)\ln(1-C) + \Omega C(1-C)]. \tag{5}$$

Here g_{A} and g_{B} are the excess energy when the epilayer is pure A or pure B. (In the special case that A, B and S atoms are all identical, g_{A} and g_{B} reduce to the surface energy of an unstrained one-component solid.) Due to mass conservation, the average concentration is constant when atoms diffuse within the epilayer. Consequently, in Eq. (5) the terms involving g_{A} and g_{B} do not affect diffusion. Only the function in the bracket does, which is drawn in Fig. 2. The first two terms in the bracket result from the entropy of mixing, and the third term from the energy of mixing. Λ is the number of atoms per unit area on the surface, k is Boltzmann's constant, and T is the absolute temperature. The dimensionless number Ω measures bond strength

relative to the thermal energy kT. When $\Omega<2$, the function is convex. When $\Omega>2$, the function has double wells. The $g(C)$ function drives phase separation; it favors neither coarsening nor refining.

We assume that $h(C)$ is a positive constant, $h(C)=h_0$. Any nonuniformity in the concentration field by itself increases Γ. In the phase field model, the second term in Eq. (4) represents the phase boundary energy; it drives phase coarsening.

The quantity f, known as the surface stress, is the surface energy change associated with the elastic strain (Cahn, 1980). When the concentration is nonuniform, the surface stress is also nonuniform. As stated in Section 1, this concentration-dependent surface stress drives phase refining. For simplicity, we assume that the surface stress is a linear function of the concentration, $f(C)=\psi+\phi C$. Ibach (1997) has reviewed experimental information on the concentration-dependent surface stress in various systems.

On annealing, atoms diffuse within the epilayer to reduce the free energy as defined by Eq. (1). The corresponding diffusion equation is given by (Suo and Lu, 2001)

$$\frac{\partial C}{\partial t}=\frac{M}{\Lambda^2}\nabla^2\left(\frac{\partial g}{\partial C}-2h_0\nabla^2 C+\phi\varepsilon_{\beta\beta}\right), \tag{6}$$

where M is the mobility of atoms in the epilayer. The first two terms in Eq. (6) are due to the free energy of mixing and the phase boundary energy, and are analogous to those in Cahn (1961). The third term is due to the concentration-dependent surface stress.

The nonuniform surface stress generates a traction field on the surface: $\sigma_{31}=\partial f/\partial x_1$ and $\sigma_{32}=\partial f/\partial x_2$, which, in its turn, generates an elastic field in the substrate. The elastic field in a half-space due to a tangential point force acting on the surface was solved by Cerruti (see Johnson, 1985, p. 69). A linear superposition gives the field due to the distributed traction on the surface:

$$\varepsilon_{\beta\beta}=-\frac{(1-\nu^2)\phi}{\pi E}\iint\frac{(x_1-\xi_1)\partial C/\partial\xi_1+(x_2-\xi_2)\partial C/\partial\xi_2}{[(x_1-\xi_1)^2+(x_2-\xi_2)^2]^{3/2}}\,\mathrm{d}\xi_1\,\mathrm{d}\xi_2. \tag{7}$$

The integration extends over the entire surface. Eqs. (5)–(7) govern the dynamic system. Given an initial concentration field, $C(x_1,x_2,0)$, the equations completely determine subsequent concentration field, $C(x_1,x_2,t)$. The diffusion equation is nonlinear because of the function $g(C)$, and contains both differentiation and integration.

3. Numerical algorithm

A comparison of the first two terms in the parenthesis in Eq. (6) defines a length:

$$b=\left(\frac{h_0}{\Lambda kT}\right)^{1/2}. \tag{8}$$

In the Cahn–Hilliard model this length scales the distance over which the concentration changes from the level of one phase to that of the other. Loosely speaking, one may call b the width of the phase boundary. The magnitude of h_0 is of the order of energy per atom at a phase boundary. Using magnitudes $h_0 \sim 10^{-19}\,\mathrm{J}$, $\Lambda \sim 5 \times 10^{19}\,\mathrm{m}^{-2}$ and $kT \sim 5 \times 10^{-21}\,\mathrm{J}$ (corresponding to $T = 400\,\mathrm{K}$), we have $b \sim 0.6\,\mathrm{nm}$.

The competition between coarsening and refining (i.e., between the last two terms in Eq. (6)) defines another length:

$$l = \frac{Eh_0}{(1-\nu^2)\phi^2}. \tag{9}$$

Young's modulus of a bulk solid is about $E \sim 10^{11}\,\mathrm{N/m^2}$. According to Ibach (1997), the slope of the surface stress is of the order $\phi \sim 4\,\mathrm{N/m}$. These magnitudes, together with $h_0 \sim 10^{-19}\,\mathrm{J}$, give $l \sim 0.6\,\mathrm{nm}$. The following numerical simulation shows that the equilibrium phase size is of the order $\sim 4\pi l$. This broadly agrees with experimentally observed phase sizes.

From Eq. (6), disregarding a dimensionless factor, we note that the diffusivity scales as $D \sim MkT/\Lambda$. To resolve events occurring over the length scale of the phase boundary width, b, the time scale is $\tau = b^2/D$, namely,

$$\tau = \frac{h_0}{M(kT)^2}. \tag{10}$$

Normalize the coordinates x and ξ by b, and the time t by τ. In terms of the dimensionless coordinates and time, Eqs. (5)–(7) are combined into

$$\frac{\partial C}{\partial t} = \nabla^2 \left\{ P(C) - 2\nabla^2 C - \frac{Q}{\pi} \iint \frac{(x_1-\xi_1)\partial C/\partial \xi_1 + (x_2-\xi_2)\partial C/\partial \xi_2}{[(x_1-\xi_1)^2+(x_2-\xi_2)^2]^{3/2}} \mathrm{d}\xi_1\,\mathrm{d}\xi_2 \right\}, \tag{11}$$

where $Q = b/l$ and

$$P(C) = \ln\left(\frac{C}{1-C}\right) + \Omega(1-2C). \tag{12}$$

Solving Eq. (11) by finite difference in real space is inefficient. For example, a typical calculation of 256×256 grids on a 300 MHz SGI workstation takes more than half a month for the system to evolve to $t = 10^5$ (normalized time) with time step $\Delta t = 1$. A better method is to solve the equation by the Fourier transformation (Wang et al., 1993). Denote the Fourier transform of $C(x_1, x_2, t)$ by $\hat{C}(\alpha, \beta, t)$, where α and β are the coordinates in the reciprocal space. That is,

$$\hat{C}(\alpha, \beta, t) = \int_{-\infty}^{\infty}\int_{-\infty}^{\infty} C(x_1, x_2, t) \mathrm{e}^{-\mathrm{i}(\alpha x_1 + \beta x_2)}\,\mathrm{d}x_1\,\mathrm{d}x_2. \tag{13}$$

Regard P as a function $P(x_1, x_2, t)$, and transform it to $\hat{P}(\alpha, \beta, t)$. Take the Fourier transform on both sides of Eq. (11), and we obtain that

$$\frac{\partial \hat{C}}{\partial t} = -k^2\hat{P} - 2(k^4 - k^3 Q)\hat{C}, \tag{14}$$

where $k=\sqrt{\alpha^2+\beta^2}$. Because $P(C)$ is a nonlinear function, amplitudes $\hat{C}$ for various modes (α,β) are coupled.

Another concern in the numerical simulation is the time variable in Eq. (14). The explicit forward Euler method requires very small time step to maintain stability. Instead, we adopt the semi-implicit scheme proposed by Chen and Shen (1998). Treat the linear term implicitly to reduce the stability constraint, while still treat the nonlinear term explicitly to avoid solving nonlinear equations at each time step. For a given time t and a time step Δt, denote $\hat{C}^n=\hat{C}(\alpha,\beta,t)$, $\hat{P}^n=\hat{P}(\alpha,\beta,t)$, and $\hat{C}^{n+1}=\hat{C}(\alpha,\beta,t+\Delta t)$. In Eq. (14) replace $\hat{C}$ by $\hat{C}^{n+1}$, $\partial\hat{C}/\partial t$ by $(\hat{C}^{n+1}-\hat{C}^n)\Delta t$, and $\hat{P}$ by $\hat{P}^n$. We obtain that

$$\hat{C}^{n+1}=\frac{\hat{C}^n-k^2\hat{P}^n\Delta t}{1+2(k^4-k^3Q)\Delta t}. \tag{15}$$

This equation is valid for any α and β.

We restrict the simulation in a square cell of size $L\times L$ in the real space (x_1,x_2). The periodic boundary condition is applied to replicate the cell to the entire surface. The cell size must be large enough to contain sufficient numbers of features, but small enough to shorten the computation time. Linear perturbation analysis (Lu and Suo, 1999) estimates the equilibrium wavelength to be $4\pi l$. In our simulation, we choose the cell size of the order $L\sim 200\,l$. The cell is divided into $N\times N$ grids. The grid space, $\Delta=L/N$, should be small enough to describe the phase boundary. We choose $\Delta=b$ in our simulation.

The corresponding calculation cell in the reciprocal space (α,β) is of size $2\pi/\Delta\times 2\pi/\Delta$. The cell is also divided into $N\times N$ grids, with grid space $2\pi/L$. The discrete Fourier transform connects the values of C and P at the grid points in the real space to those of $\hat{C}$ and $\hat{P}$ at the grid points in the reciprocal space. The fast Fourier transformation (FFT) is applied.

The input comprises the initial concentration distribution, as well as the parameters Q and Ω. At each time step, calculate P^n from C^n according to Eq. (12) at every grid point in the real space. Then transform the values of C^n and P^n at all the grid points in the real space to those of $\hat{C}^n$ and $\hat{P}^n$ in the reciprocal space. Update to $\hat{C}^{n+1}$ according to Eq. (15) at every grid point in the reciprocal space. Apply the inverse FFT to $\hat{C}^{n+1}$ to obtain the concentration field C^{n+1} in the real space. Repeat the above procedure for the next time step.

The balance between coarsening and refining affects the phase size. In our simulation, the balance is controlled through the dimensionless number Q, which is set to be $Q=1$. We set $\Omega=2.2$; the corresponding $g(C)$ is a double-well function shown in Fig. 2 with $C_1=0.249$ and $C_2=0.751$. The calculation cell contains 256×256 grids with grid size $\Delta=b$. The time step $\Delta t=0.4\tau$. The simulation is performed on a 300 MHz SGI workstation. A calculation to $t=10^6\tau$ takes about one week. We visualize the evolving patterns in the real space, plotting the concentration levels at a given time in a gray scale.

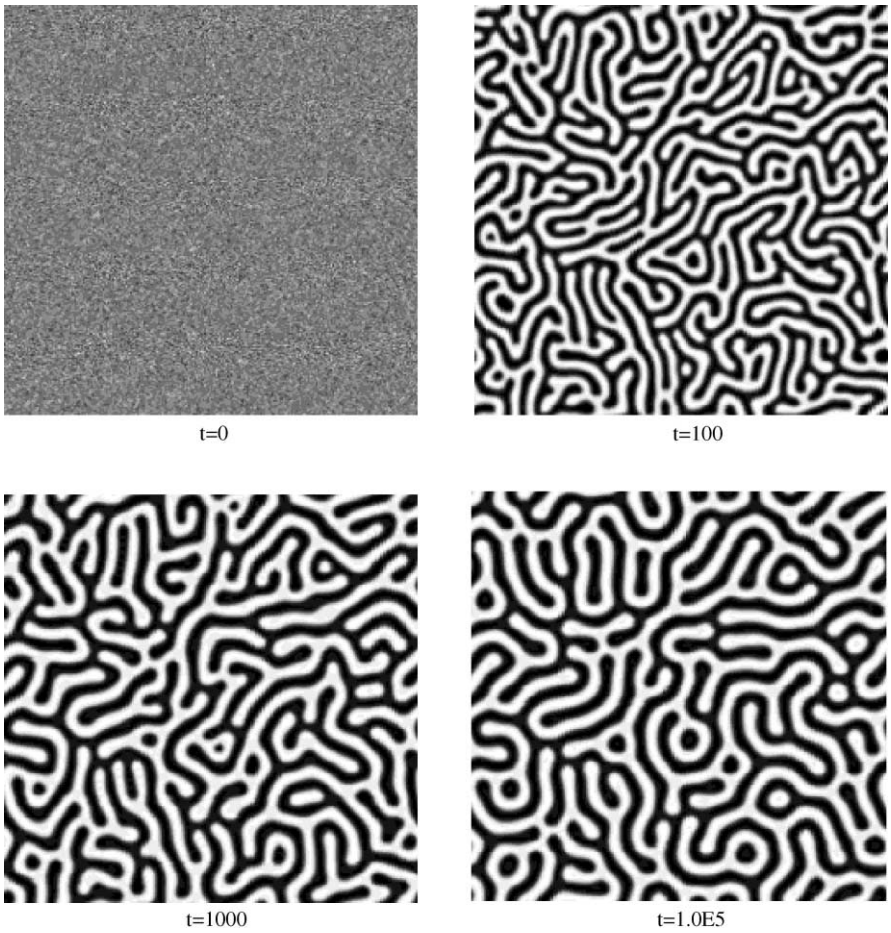

Fig. 3. Simulation starts with a random initial condition. The average concentration equals 0.5.

4. Results

4.1. Serpentine structure

Fig. 3 shows an evolution sequence at four times, given in units of τ. The average concentration is $C_{\text{ave}} = 0.5$. The initial condition is set to fluctuate randomly within 0.001 from the average. When the simulation starts, all processes are concurrent. However, it may be convenient to note three stages in the evolution. The early stage involves mainly the amplification of fluctuations. The amplitude of the concentration rapidly attains the values equal to the equilibrium composition. In the intermediate stage, the phases coarsen. The phases exhibit an interwoven, connected morphology, which is common in spinodal decomposition. Unlike spinodal decomposition, however,

the phases in the epilayer will not coarsen forever since the surface stress provides a refining effect. Observe that from $t = 10^3$ to 1.0×10^5 the phase size is almost invariant. In the late stage of the evolution, the serpentine structure tries to line up into stripes. However, this process is very slow. The system is isotropic: the stripes are confused, not knowing which direction to prefer. The serpentine structures have been observed in many self-assembled systems, including block coploymers (e.g., Park et al., 1997), ferromagnetic films (e.g., Giess, 1980), and Langmuir monolayers (e.g., Seul and Chen, 1993).

4.2. Forming stripes by breaking symmetry

One can remove the confusion by breaking the symmetry. Fig. 4 shows another evolution sequence at eight times. On top of the same random initial condition we added three lines, each 3Δ wide and having concentration $C = 0.51$. The three lines provide a direction to line up the stripes. Observe that concentration waves expand from the three lines and form "seeds" of superlattices. These seeds grow into stripe colonies by consuming the nearby serpentine structures.

At $t = 100$, when two stripe colonies meet, an irregular region emerges, reminiscent of dislocations in atomic crystals. At $t = 500$, well-defined dislocations form. Each dislocation moves by climbing; the mass of a dislocation diffuses to its neighbors. The phenomenon is captured from $t = 500$ to 1000. We obtain periodic stripes in the entire calculation cell within $t = 10^5$. The present simulation suggests that serpentine structures can transform into an array of stripes if one breaks the symmetry at a coarse scale, e.g., by phopolithography.

4.3. Densely packed dots

Fig. 5 shows an evolution sequence of a simulation with the average concentration $C_{\text{ave}} = 0.4$. The calculation starts from a random initial condition. The epilayer forms dots instead of stripes. One can broadly identify three stages of evolution. In the early stage, the concentration rapidly attains the two equilibrium compositions. In the intermediate state, the dots approach to equilibrium size and form domains. In each domain the dots order into a triangular lattice. The dots at the domain boundary are less ordered, and have excess energy relative to those inside the domains. In the late stage, the dots tend to rearrange themselves to form a superlattice of long-range order. However, the rearrangement takes much longer time than setting the dot sizes. In spinodal decomposition of a bulk alloy, the late stage evolution is characterized by coarsening: large particles grow larger and small particles disappear. In an epilayer, the late stage involves rearrangement of dots with their size invariant.

Dots with local order and polydomains have been observed in many self-assembled two-dimensional systems, including block coploymers and Langmuir monolayers. Long-range ordering is difficult to attain. Similar phenomenon appears in the recently discovered lithographically induced self-assembly (LISA) (Chou and Zhuang, 1999). However, these authors showed that by using a combination of lithography and self-assembly, a wide range of patterns can be obtained.

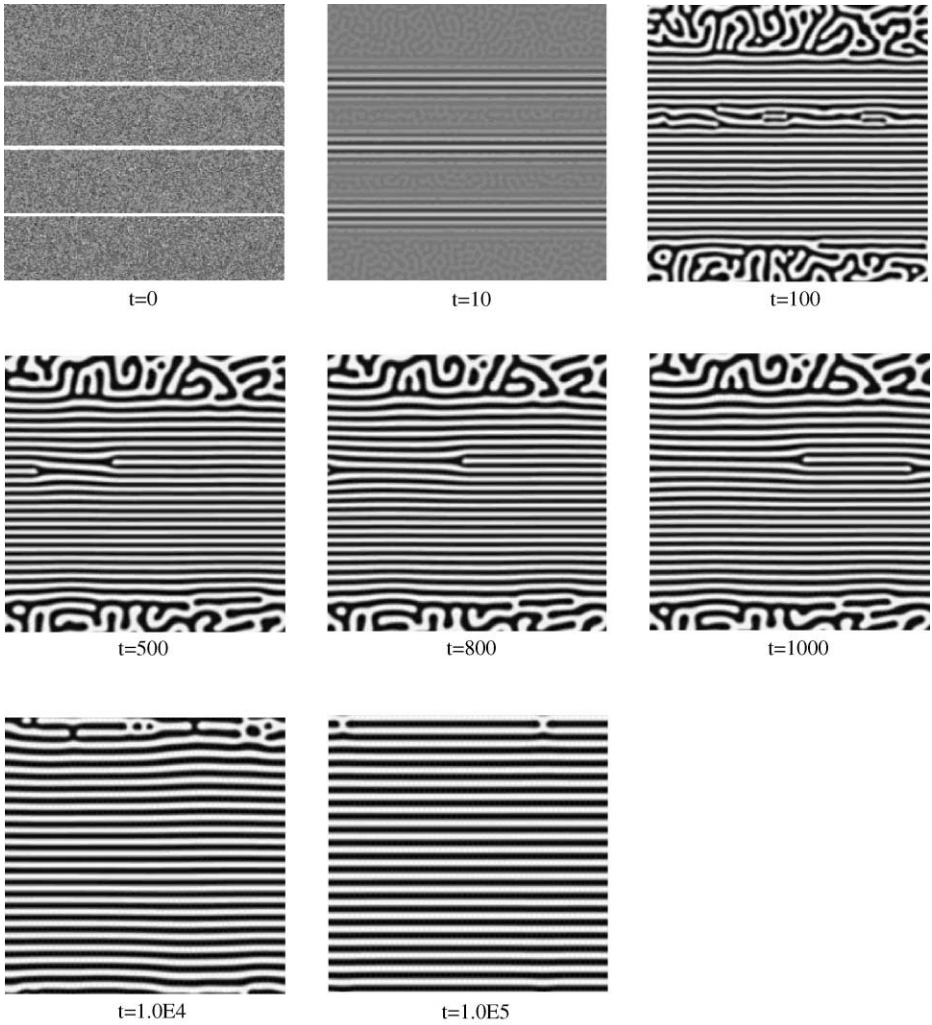

Fig. 4. Simulation starts with a random initial condition plus three lines with $C = 0.51$. The average concentration equals 0.5.

4.4. *Effects of material anisotropy*

In addition to the anisotropy in initial condition, another way to break the symmetry is to invoke material anisotropy. Fig. 6 gives the snap shots of the evolution for a system in which the phase boundary energy is anisotropic. In the simulation, the value of h in the x_1 direction is 0.9 times of that in the x_2 direction. The diffusion equation is modified accordingly. Consequently, the stripes tend to form along the

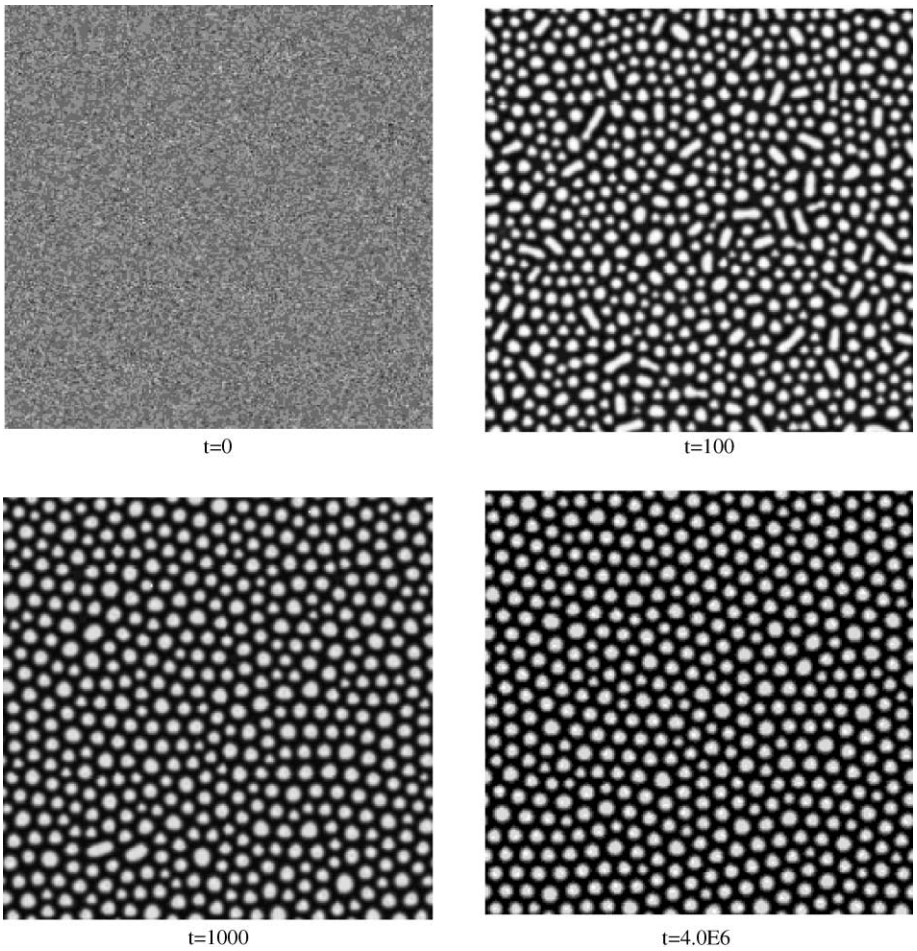

Fig. 5. Simulation starts with a random initial condition. The average concentration equals 0.4.

x_2 direction. Presumably, the oxide stripes on the (1 1 0) Cu surface are due to such anisotropy.

Fig. 7 shows a sequence with $C_{ave} = 0.4$. The value of h in the x_1 direction is half that in the x_2 direction. The initial concentration field is disordered. The material anisotropy causes the epilayer to form stripes. Recall that for an isotropic system, an epilayer with $C_{ave} = 0.4$ forms dots as shown in Fig. 5.

5. Concluding remarks

The formation of stable concentration pattern in an epitaxial monolayer requires three ingredients: phase separation, phase coarsening, and phase refining. The

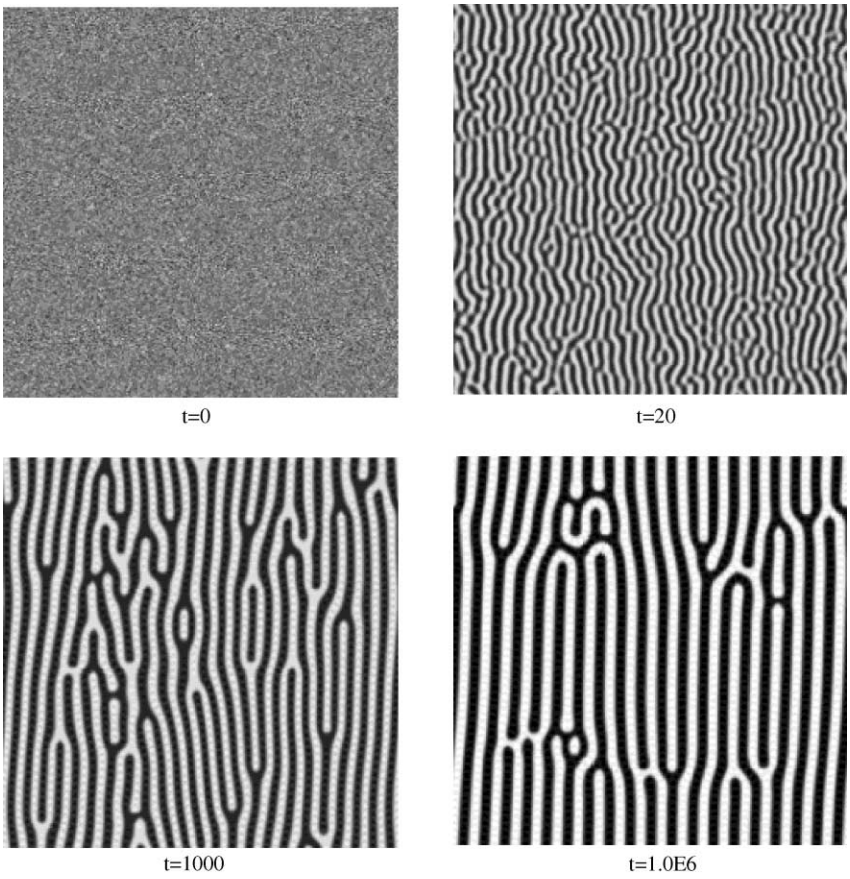

Fig. 6. Simulation starts with a random initial condition. $C_{ave} = 0.5$. The value of h in the x_1 direction is 0.9 times of that in the x_2 direction.

continuous phase field model represents phase separation with a double-well free energy of mixing, phase coarsening with a concentration gradient term in the surface energy, and phase refining with a concentration-dependent surface stress. These ingredients result in a nonlinear diffusion equation, which is solved numerically by using the fast Fourier transformation and a semi-implicit method. Starting with a disordered initial concentration field, an epilayer evolves into a serpentine structure when the average concentration is close to 0.5, or densely packed dots when the average concentration is somewhat below 0.5. For the case that $C_{ave} = 0.5$, the self-assembly into stripes is accelerated by introducing a few straight lines in the initial condition, or invoking anisotropy in materials. With suitable "seeding" (e.g., by lithography at a coarse scale), one may form coarse patterns of self-assembled superlattices. This exciting possibility will be studied further in subsequent work.

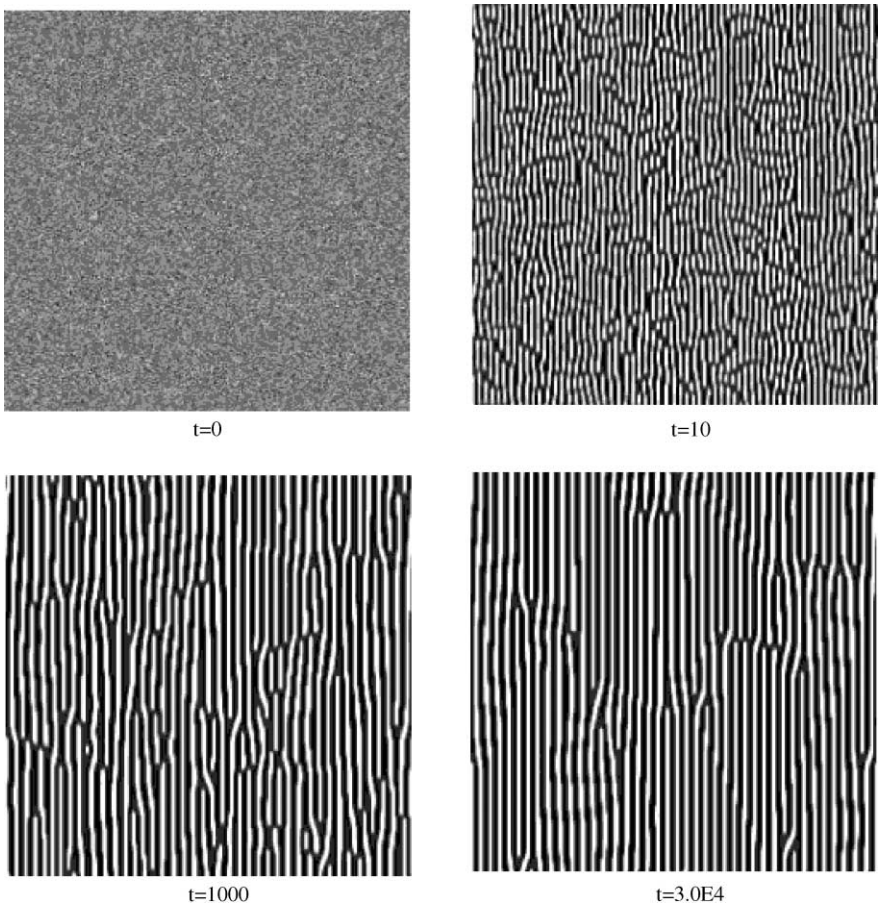

Fig. 7. Simulation starts with a random initial condition. $C_{ave} = 0.4$. The value of h in the x_1 direction is 0.5 times of that in the x_2 direction.

Acknowledgements

This work is supported by the Department of Energy through contract DE-FG02-99ER45787.

References

Alerhand, O.L., Vanderbilt, D., Meade, R.D., Joannopoulos, J.D., 1988. Spontaneous formation of stress domains on crystal surfaces. Phys. Rev. Lett. 61, 1973–1976.

Cahn, J.W., 1961. On spinodal decomposition. Acta Metall. 9, 795–801.

Cahn, J.W., 1980. Surface stress and the chemical equilibrium of small crystals—I. the case of the isotropic surface. Acta Metall. 28, 1333–1338.

Cahn, J.W., Hilliard, J.E., 1958. Free energy of a nonuniform system. I. Interfacial free energy. J. Chem. Phys 28, 258–267.

Chen, L.-Q., Khachaturyan, A.G., 1993. Dynamics of simultaneous ordering and phase separation and effect of long-range coulomb interactions. Phys. Rev. Lett. 70, 1477–1480.

Chen, L.-Q., Shen, J., 1998. Applications of semi-implicit Fourier-spectral method to phase field equations. Comp. Phys. Commun. 108, 147–158.

Chen, L.-Q., Wang, Y., 1996. The continuum field approach to modeling microstructural evolution. JOM 48, 13–18.

Chou, S.Y., Zhuang, L., 1999. Lithographically-induced self-assembly of periodic polymer micropillar arrays. J. Vac. Sci. Tech. B 17, 3197–3202.

Clark, P.G., Friend, C.M., 1999. Interface effects on the growth of cobalt nanostructures on molybdenum based substrates. J. Chem. Phys. 111, 6991–6996.

Giess, E.A., 1980. Magnetic-bubble materials. Science 208, 938–943.

Ibach, H., 1997. The role of surface stress in reconstruction, epitaxial growth and stabilization of mesoscopic structures. Surf. Sci. Rep. 29, 193–263.

Johnson, K.L., 1985. Contact Mechanics. Cambridge University Press, UK.

Kern, K., Niebus, H., Schatz, A., Zeppenfeld, P., George, J., Comsa, G., 1991. Long-range spatial self-organization in the adsorbate-induced restructuring of surfaces: Cu{110}-(2 × 1)O. Phys. Rev. Lett. 67, 855–858.

Lu, W., Suo, Z., 1999. Coarsening, refining, and pattern emergence in binary epilayers, in the Fred Lange Festschrift on the occasion of his 60th birthday. Z. Metallkunde 90, 956–960.

Ng, K.-O., Vanderbilt, D., 1995. Stability of periodic domain structures in a two dimensional dipolar model. Phys. Rev. B 52, 2177–2183.

Park, M., Harrison, C., Chaikin, P.M., Register, R.A., Adamson, D.H., 1997. Block copolymer lithography: periodic arrays of $\sim 10^{11}$ holes in 1 square centimeter. Science 276, 1401–1404.

Pohl, K., Bartelt, M.C., de la Figuera, J., Bartelt, N.C., Hrbek, J., Hwang, R.Q., 1999. Identifying the forces responsible for self-organization of nanostructures at crystal surfaces. Nature 397, 238–241.

Röder, H., Schuster, R., Brune, H., Kern, K., 1993. Monolayer-confined mixing at the Ag–Pt(111) interface. Phys. Rev. Lett. 71, 2086–2089.

Seul, M., Chen, V.S., 1993. Isotropic and aligned stripe phases in a monomolecular organic film. Phys. Rev. Lett. 70, 1658–1661.

Suo, Z., Lu, W., 2000. Composition modulation and nanophase separation in a binary epilayer. J. Mech. Phys. Solids 48, 211–232.

Suo, Z., Lu, W., 2001. Self-organizing nanophases on a solid surface. In: Chuang, T.J. (Ed.), Multi-scale Deformation and Fracture in Materials and Structures, a volume dedicated to Professor James R. Rice on the occasion of his 60th birthday, Kluwer Academic Publishers, Dordrecht, in press.

Wang, Y.Z., Chen, L.Q., Khachaturyan, A.G., 1993. Kinetics of strain-induced morphological transformation in cubic alloys with a miscibility gap. Acta Metall. Mater. 41, 279–296.